Journal of Power Sources 180 (2008) 791–796

Contents lists available at ScienceDirect

Journal of Power Sources

journal homepage: www.elsevier.com/locate/jpowsour

Short communication

Anodic behavior of high nitrogen-bearing steels in PEMFC environments

Heli Wang*, John A. Turner

National Renewable Energy Laboratory, Hydrogen Technologies and Systems Center, 1617 Cole Boulevard, Golden, CO 80401, USA

ARTICLE INFO

Article history:
Received 7 February 2008
Received in revised form 26 February 2008
Accepted 27 February 2008
Available online 18 March 2008

Keywords:
Stainless steel
Bipolar plate
PEMFC
XPS
Corrosion
Fuel cell

ABSTRACT

High nitrogen-bearing stainless steels, AISI Type 201 and AL219, were investigated in simulated polymer electrolyte membrane fuel cell (PEMFC) environments to assess the use of these materials in fuel cell bipolar plate applications. Both steels exhibit better corrosion behavior than 316L steel in the same environments. Type 201 steel shows similar but lower interfacial contact resistance (ICR) than 316L, while AL219 steel shows higher ICR than 316L.

X-ray photoelectron spectroscopy (XPS) analysis shows that the air-formed films on Type 201 and AL219 are composed of iron oxides, chromium oxide, and manganese oxide. Iron oxides dominate the composition of the air-formed film, specially the outer layer. Chromium oxide dominates passive films. Surface film thicknesses were estimated. The results suggest that high nitrogen-bearing stainless steels are promising materials for PEMFC bipolar plates.

1. Introduction

Stainless steels are widely accepted as leading polymer electrolyte membrane fuel cell (PEMFC) bipolar plate candidates [1–11]. They have good mechanical strength, high chemical stability, the possibility for very high production volumes, a wide range of alloy choices, and a relatively low cost, which makes them the material of choice for automotive fuel cell applications.

Most of the research on these alloys focuses on the 300 series of austenite stainless steels which have an approximate composition of Fe–18Cr–8Ni. A typical alloy is type 316 steel. In this class of stainless steel, Cr acts as the passivating element and Ni is the principal austenite forming/stabilizing element [12,13]. Mo is added to increase the corrosion resistance, especially the pitting resistance. Previous investigations in our laboratory showed that type 349 stainless steel exhibited superior corrosion resistance in simulated PEMFC environments [9]. However, cost considerations lead to a search for lower-cost alternatives, particularly a stainless steel with similar properties, but with lower nickel content. One solution is to substitute Ni with substantial amounts of Mn, another austenite former. In such alloys, nitrogen – a powerful austenite stabilizer and strengthener – is introduced to improve the corrosion resistance (especially the pitting resistance) due to the different formation mechanism between Ni and Mn.

Nitrogen represents an economically and environmentally attractive alloying element. Nitrogen alloying increases the corrosion resistance of different stainless steels in many environments. The beneficial effects of nitrogen on stainless steels include assisting the passivation of stainless steel in H_2SO_4 solutions [14], increasing the pitting resistance, and the re-passivation of 316L stainless in neutral and acidic solutions [15,16]. Getting significant amounts of nitrogen into the bulk steel is difficult. Higher levels of N alloying can be obtained with higher Mn content, however, a high level of Mn alloying (20%) is detrimental towards pitting corrosion [15,16]. Thermally nitrided AISI446 steel with a discontinuous mixture of surface nitrides and oxide provides excellent interfacial conductivity while maintaining the excellent corrosion resistance of the bare alloy [17]. This result points to the importance of nitrogen on the surface conductivity. If a steel alloy could contain more nitrogen, then the surface might be modified with nitrogen and the alloy might contain properties similar to the surface nitrided ones.

High N stainless steels are commercially available. Type 201 and AL219 alloys contain substantial amounts of Mn and less Ni than the typical 18Cr–8Ni grade steel. Compared to the 300 series alloys, the low-Ni 200 series alloys offer an economical way to obtain superior mechanical properties. With Mn and N used as partial, low-cost substitutes for Ni, these alloys become more economical and have properties similar to the high Ni alloys. These alloys have been designed specially to provide sufficient austenite stability for low temperature service. Type 201 has similar corrosion resistance to that of 304 and 304L, while AL219 is similar to that of 316. These alloys can also provide advantages over the 18-8 grades in certain

* Corresponding author. Tel.: +1 303 275 3858; fax: +1 303 275 2905.
E-mail address: heli_wang@nrel.gov (H. Wang).

0378-7753/$ – see front matter © 2008 Elsevier B.V. All rights reserved.
doi:10.1016/j.jpowsour.2008.02.085

Table 1
Chemical composition of the N-bearing steels, wt%, Fe-balance

Alloy	C	N	Cr	Ni	Mn	Mo	Si	Other
201	.084	0.067	16–18	3.5–5.5	5.5–7.5	–	1.0 max	
AL219	.022	0.315	21.0	6.00	9.00	.05	0.25	
316L	≤.028	.020–.040	16.20–16.80	10.10–10.30	1.70–1.95	2.03–2.25	.45–.65	≤.50 Cu

applications. If they could be applied to PEMFC bipolar plates, the lower cost would be a big advantage.

2. Experimental

2.1. Materials and electrochemistry

Stainless steel plates of Type 201 and AL219 were provided by Allegheny Ludlum Co. Table 1 lists their chemical compositions in weight percentage, where 316L is used for comparison purposes. Steel plates were cut into samples of 2.54 cm × 1.27 cm, polished with #600 SiC abrasive paper, rinsed with acetone, and dried with nitrogen gas. The detailed electrode fabrication procedure is described elsewhere [9–11].

To simulate an aggressive PEMFC environment, all electrochemical experiments were carried out in 1 M H_2SO_4 + 2 ppm F^- solutions at 70 °C. The temperature of the solution was controlled by a bath. The solution was purged either with hydrogen gas (to simulate PEMFC anode environment) or with pressured air (to simulate PEMFC cathode environment) prior to and during the measurements.

A conventional three-electrode system was used for the electrochemical measurements, with a saturated calomel electrode (SCE) as the reference electrode and a platinum sheet as the counter electrode. All potentials will be referred to the SCE unless otherwise noted. A Solartron 1287, controlled by a computer, was used to carry out these measurements. During dynamic polarization, the electrode was stabilized at open circuit potential (OCP) for 5 min and the potential was then scanned from OCP to the anodic direction with a rate of 1 mV s^{-1}. During potentiostatic polarization, the electrode was also stabilized for 5 min. A specific potential was then applied and the current was recorded.

2.2. Interfacial contact resistance (ICR)

All ICR measurements were carried out at room temperature with dry samples. The method for ICR measurements has been previously described [9]. In short, two pieces of carbon papers were sandwiched between the stainless steel sample and the two copper plates. A current of 1.000 A was provided via the two copper plates and the total voltage drop was recorded as the compaction force increased gradually. During the measurement, a voltage drop was recorded about ~2 min after this drop was stabilized. We then calculated the dependence of total resistance on the compaction force. The ICR value of the carbon paper/copper plate interface ($R_{C/Cu}$) was determined by a calibration. Therefore, we report only the corrected ICR values for the carbon paper/stainless steel interface ($R_{C/SS}$).

2.3. XPS characterization

X-ray photoelectron spectroscopy (XPS) was used to investigate the air-formed film and characterize the passive film after polarization in the PEMFC environments. The procedure for the XPS measurements is described elsewhere [18]. In short, measurements were carried out in a Phi 5600 electron spectrometer using Al Kα radiation X-ray source (1486.6 eV) and a hemispherical energy analyzer. The base pressure in the spectrometer chamber was 1.33×10^{-8} Pa. The depth profiles were obtained by sputtering the samples with 3 keV argon ions. During the sputtering, the pressure in the chamber was 6.67×10^{-5} Pa. The sputtering rate was as 38 Å min^{-1}. Due to the roughness of the sample surface, the XPS analysis could only give qualitative analysis about the surfaces.

3. Results and discussion

3.1. Polarization behavior of stainless steels

Dynamic polarizations for the chosen steels in 1 M H_2SO_4 + 2 ppm F^- at 70 °C, purged with hydrogen gas, are shown in Fig. 1. As a comparison, 316L steel shows a typical polarization curve, which is passivated at *ca.* −0.25 V and experiences trans-passivation at *ca.* 0.9 V. Lowest current in the passivation range for 316L is *ca.* 13 μA cm^{-2}. We observed that the polarization curves for Type 201 and AL219 steels are similar. However, both are more complicated than and different from the polarization curve for 316L. Passivation occurs at *ca.* −0.27 V for Type 201 and *ca.* −0.37 V for AL219 steel. In the polarization curves, secondary passivation peaks are registered at *ca.* −0.05 V for Type 201 and *ca.* −0.06 V for AL219 steels. Trans-passivation occurs at *ca.* 0.8 V for both Type 201 and AL219 steels. Lowest current in the passivation range is *ca.* 8.6 μA cm^{-2} for Type 201 and *ca.* 5.6 μA cm^{-2} for AL219 steel, both are lower than that for 316L. Fig. 1 suggests that AL219 steel has a higher passivating ability than the rest.

When the solution is purged with air, the resulting dynamic polarization curves are displayed in Fig. 2. Again, 316L is passivated at *ca.* −0.2 V and trans-passivated at *ca.* 0.9 V. Complex passivation processes are observed with Type 201 and AL219 steels. Fig. 2 shows that primary passivation occurs at *ca.* −0.28 V for Type 201 and *ca.* −0.37 V for AL219. Secondary passivation peaks are registered for both alloys. They are at *ca.* −0.14 V and −0.05 V for Type 201 steel, and *ca.* −0.18 V and −0.04 V for AL219 steel. Trans-passivation occurs at *ca.* 0.8 V, independent of the purged gas. At 0.6 V, all three

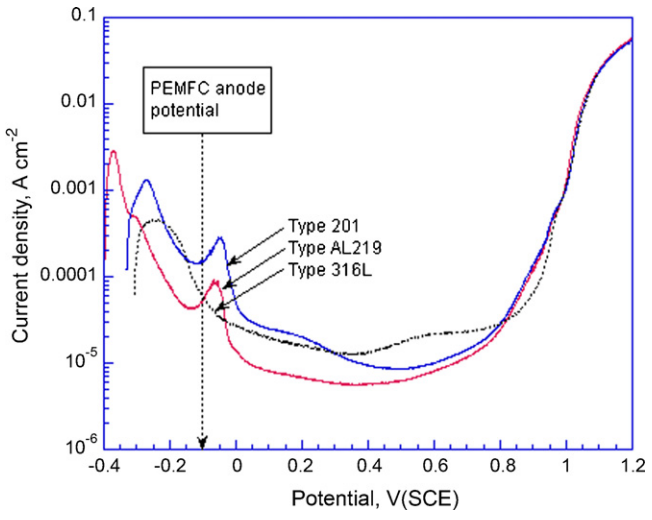

Fig. 1. Dynamic polarization of steels in 1 M H_2SO_4 + 2 ppm F^- at 70 °C. The scan rate was 1 mV s^{-1} and the solution was purged with hydrogen gas.

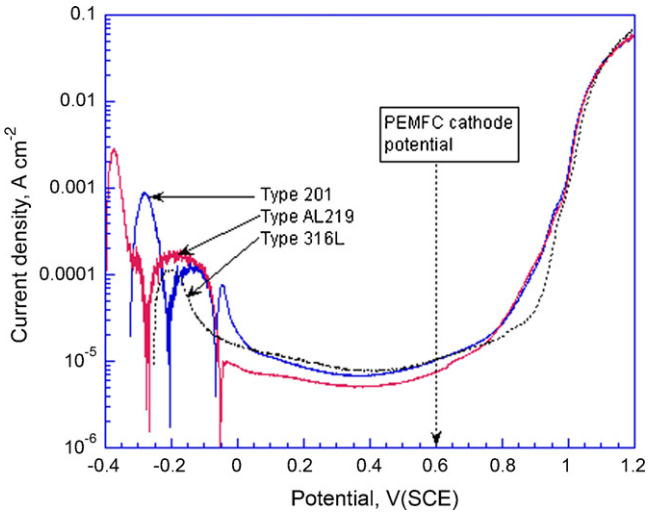

Fig. 2. Dynamic polarization of steels in 1 M H_2SO_4 + 2 ppm F^- at 70 °C. The scan rate was 1 mV s^{-1} and the solution was purged with air.

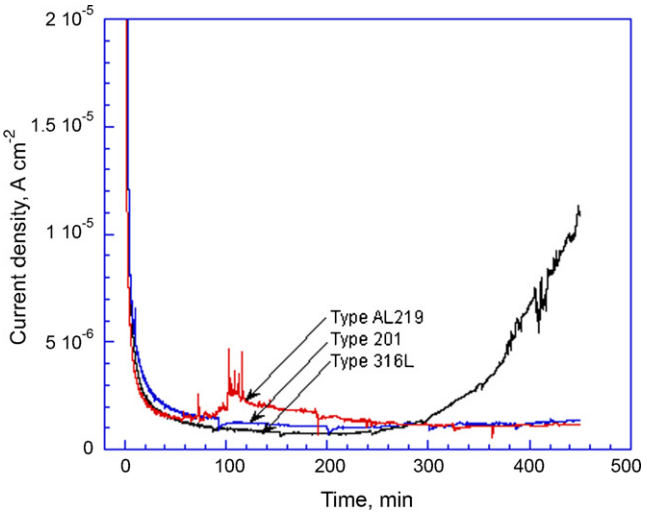

Fig. 4. Anodic behavior of steels at 0.6 V in 1 M H_2SO_4 + 2 ppm F^- at 70 °C. The solution was purged with air.

steels are in the passivation region and low currents are obtained.

The complicated polarization curves in Figs. 1 and 2, specially the secondary peaks during passivation for Type 201 and AL219 alloys should be related to their high nitrogen contents. Similar peaks were registered for high N-bearing 301LN steels in 10% H_2SO_4 solution [19], though the authors did not give a clear explanation. Referring to the previous work about N-containing stainless steels by Clayton and co-workers [20,21], it is considered that the secondary peaks in Figs. 1 and 2 could be due to the surface nitrides/surface ammonia formation, though more work is needed to understand the details.

Fig. 3 shows the potentiostatic polarization at −0.1 V in hydrogen-purged solution. 316L steel shows a slight increase in the anodic current during the tested period reaching approximately 12 μA cm^{-2} at the end of the test. An anodic to cathodic current transition occurred with Type 201 steel, which then goes back anodic, reaching to approximately 8.0 μA cm^{-2} at the end of the test. This confirms the beneficial effect of nitrogen for the alloy in PEMFC anode environment. AL219 steel shows a cathodic current for the whole period, indicating that the steel's surface is cathodically protected and the corrosion rate is very low. The current is approximately −3.0 μA cm^{-2} and very stable. This is promising for PEMFC bipolar plate applications. The behavior from the potentiostatic polarizations agrees well with the steels' dynamic polarization. The results of the anodic behavior of the steel when polarized at 0.6 V and the solution is purged with air, is shown in Fig. 4. 316L steel shows a sharp current increase after approximately 250 min of polarization, reaching about 11 μA cm^{-2} at the end of the test. A small current peak is seen with AL219L at approximately 100 min of polarization and this peak has a very low value of a few μA cm^{-2}. Type 201 steel shows the best stability in this set, although the behavior of AL219 is very good. The performance of Type 201 steel in PEMFC environments is very promising from an economical point of view. In the long run, AL219 seems better than Type 201, so, in view of the corrosion resistance in PEMFC environments, AL219 is a good candidate for bipolar plate applications.

3.2. ICR

The ICRs of the two high nitrogen-bearing steels are shown in Fig. 5. 316L is also shown for comparison. It is interesting to note

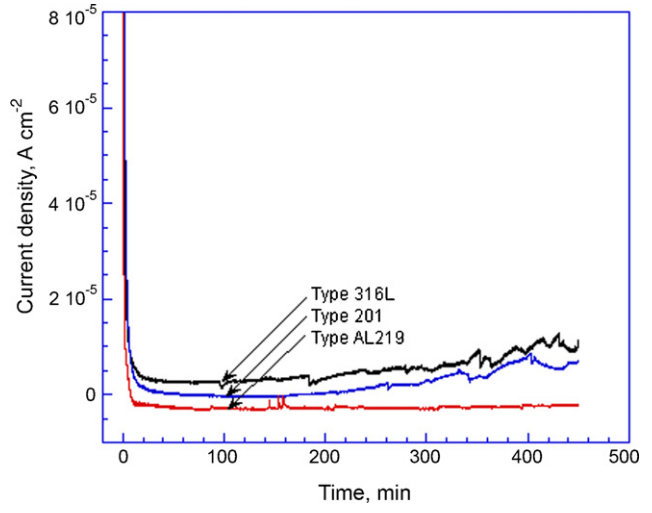

Fig. 3. Anodic behavior of steels at −0.1 V in 1 M H_2SO_4 + 2 ppm F^- at 70 °C. The solution was purged with hydrogen gas.

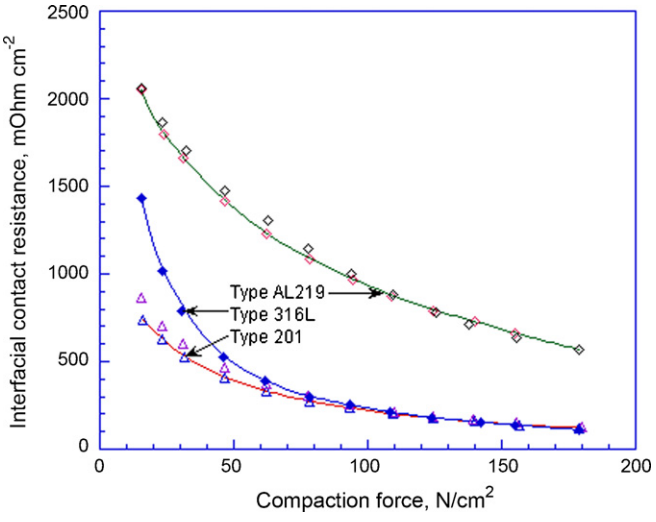

Fig. 5. Interfacial contact resistance of high nitrogen-bearing steels. ICR values for 316L are plotted for comparison.

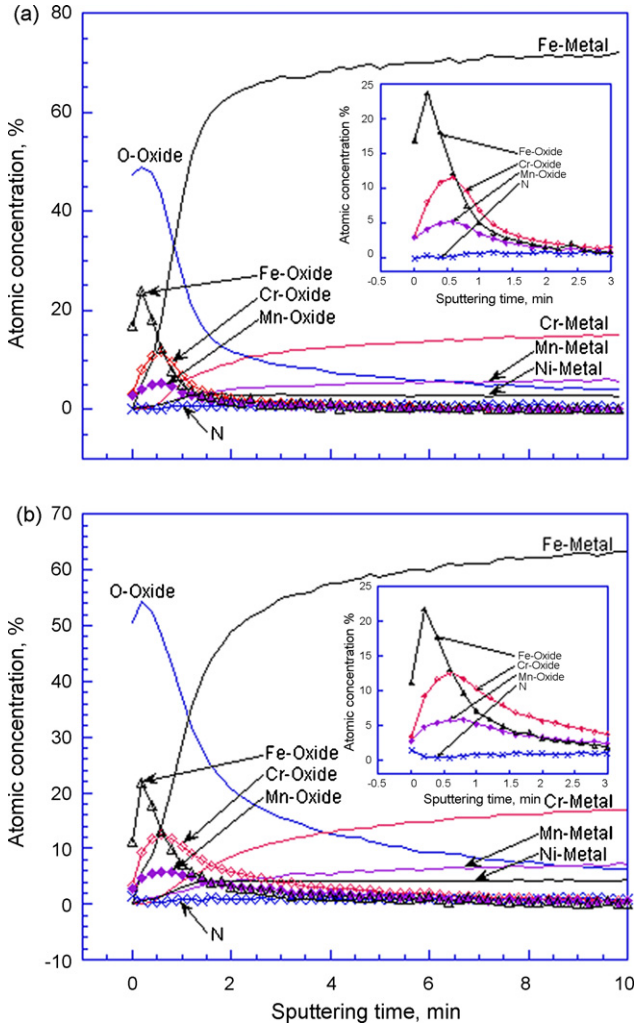

Fig. 6. XPS depth profiles for Type 201 steel (a) and AL219 steel (b) with air-formed oxide films.

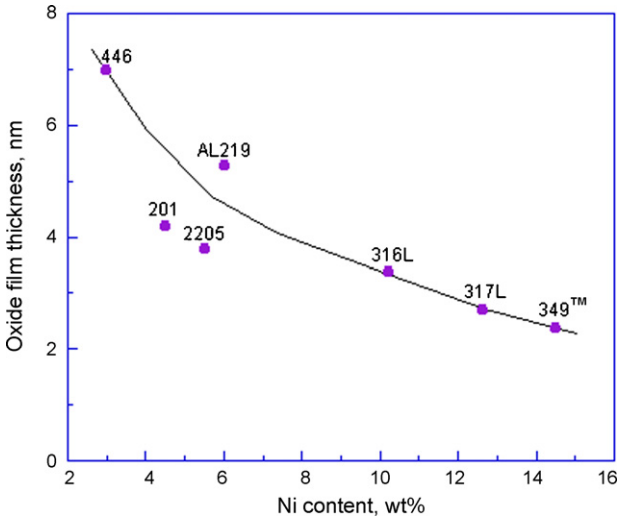

Fig. 7. Dependence of air-formed oxide film thickness on the nickel content of stainless steels.

that the ICRs of the Type 201 steel are in the same level as 316L steel for compaction forces over 110 N cm^{-2}. Below this compaction force range, the ICRs are even lower than those of 316L. Comparing the chemical composition of Type 201 and 316L steels, the major difference is the substitution of Mn in Type 201 steel for the Ni in 316L. This could explain the similarity of the ICR curves. Though there are other differences in the elemental compositions, the resulting effect is minor. The comparable ICR and good corrosion resistance of Type 201 steel suggests a low-cost bipolar plate candidate.

For AL219 steel, however, much higher ICR values than those of 316L are obtained. This high ICR would certainly affect the bipolar plate application of this alloy. Comparing the chemical compositions of the two, AL219 has much higher Cr than 316L. Moreover, the N and Mn contents are much higher than Type 201 steel. One might expect to have some nitrides on the surface due to the high N content, however, the nitride phase in the solid solution depends on the treatment of the steel. It is possible that non-conductive CrN might form in the matrix during the treatment of the AL219 steel. If this is the case, high ICR might result. More research is necessary to understand this surface.

3.3. *Depth profiles of the surface films*

Fig. 6 gives the XPS depth profiles for Type 201 and AL219 steels with air-formed oxide films. The insets show the film's composition

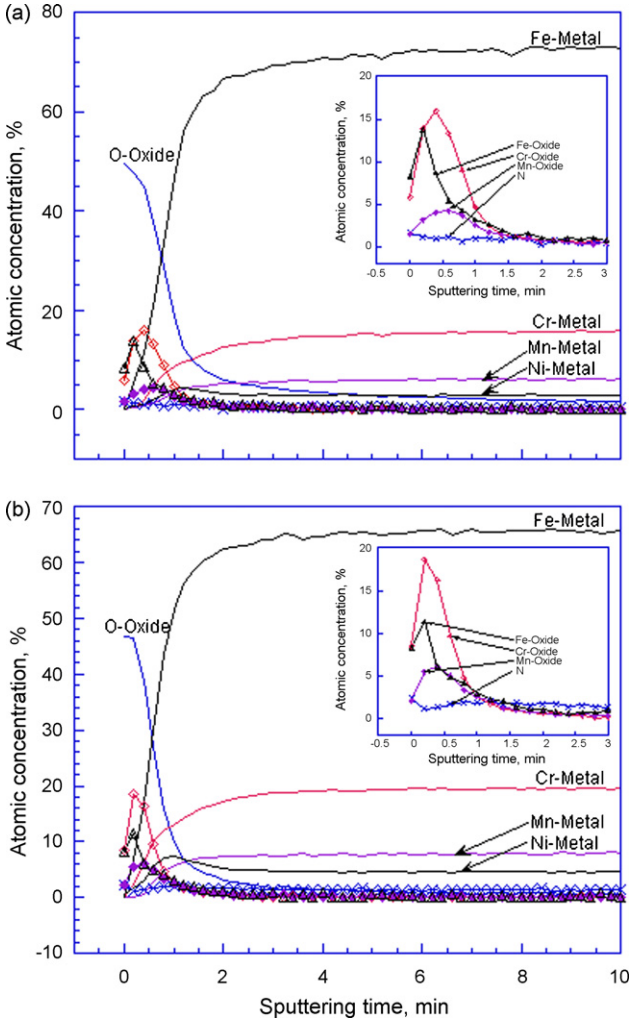

Fig. 8. XPS depth profiles for Type 201 (a) and AL219 (b) steels after polarized 7.5 h at −0.1 V in 1 M H_2SO_4 + 2 ppm F^- solution of 70 °C. The solution was purged with hydrogen gas.

for the first 3 min of sputtering. Air-formed films on 300 series, 400 series, and grade 2205 stainless steels are composed of iron oxides and chromium oxide with an iron-rich outer layer and chromium-rich inner layer [10,11,18]. For Type 201 and AL219 steels, however, iron oxides dominate the oxide surface for both steels (see insets of Fig. 6). Moreover, manganese oxide has a significant contribution to the surface film. By carefully inspecting the inset of Fig. 6(a), we see that the surface film on Type 201 steel has only one layer and iron oxides are the major constituent. In contrast, for AL219 the inset of Fig. 6(b) indicates that iron oxides dominates outer layer while chromium oxide has a major role in the inner part of the oxide film. In this regard, the air-formed oxide film on AL219 steel is similar to that of the other stainless steels [10,11,18], except for the contribution from manganese oxide. Moreover, the surface enrichment of nitrogen on AL219 is significantly different from that of the Type 201 steel. A mixture of iron oxides, chromium oxide, and manganese oxide is a good description for the air-formed film on Type 201 and AL219 steels.

Taking the half-height of the oxygen from the oxide content (O = Oxide in Fig. 6) as an estimate of the film/substrate steel interface [22], the air-formed films on Type 201 and AL219 steels require approximately 1.1 min and 1.4 min of sputtering, respectively. Adopting a sputtering rate of 38 Å min^{-1}, the air-formed films on Type 201 and AL219 stainless steels are 4.2 nm and 5.3 nm thick, respectively. They are thicker than the air-formed film on 349 steel (2.4 nm) [18], thinner than the air-formed film on AISI446 steels (7.0 nm) [10], and in a similar range as the air-formed film on 2205 (3.8 nm) [11]. It is plausible that the thickness of the air-formed film on the stainless steel depends on the nickel content—AISI446 has the lowest nickel content, 349 has the highest, and 2205 is in the middle. To illustrate this, Fig. 7 gives the as-formed surface film thickness as a function of nickel content. A clear trend is observed: film thickness decreases with increased nickel content in the steel. It is interesting to point out that while nickel is not found in the surface film, it appears to have a major influence in controlling the thickness of the film. Clearly, detailed work is needed to understand this behavior.

The passive films formed after experimentation are also composed of iron oxides, chromium oxide, and manganese oxide. Fig. 8 gives the depth profiles for the two steels polarized at −0.1 V in the simulated PEMFC anode environment. The insets in Fig. 8 show the depth profiles of the oxides and nitrogen during the first 3 min of sputtering. In this case, however, chromium oxide dominates the passive film composition, while manganese oxide and nitrogen content in the film seem unaffected. This indicates that the passive film is different in chemical composition and nature from the air-formed film. Moreover, Fig. 8(a) and (b) reveal that chromium oxide dominates in the passive films.

Comparing the depth profiles in Fig. 6 and Fig. 8(a) and (b), we see that iron is depleted during the passivation process, resulting in the chromium-rich passive film. In other words, iron is selectively dissolved during the passivation process and chromium seems not to be depleted. This is in agreement with previous investigations in which iron was found to be depleted and chromium enriched with the austenite stainless steels and Fe–Cr alloys [23–25]. Adopting the half-height of the oxygen in oxide as the estimate of the film/substrate steel interface and a sputtering rate of 38 Å min^{-1}, the thickness of the passive films formed in the simulated PEMFC anode environment are 3.4 nm for type 201 steel and 2.7 nm for AL219 steel.

Fig. 9 shows the depth profiles of the alloys polarized at 0.6 V in the PEMFC cathode environment. Insets of Fig. 9 display the oxides and nitrogen content in the first 3 min of sputtering. Chromium oxide still dominates the passive film formed in the simulated PEMFC cathode environment. We also observed that the iron oxides

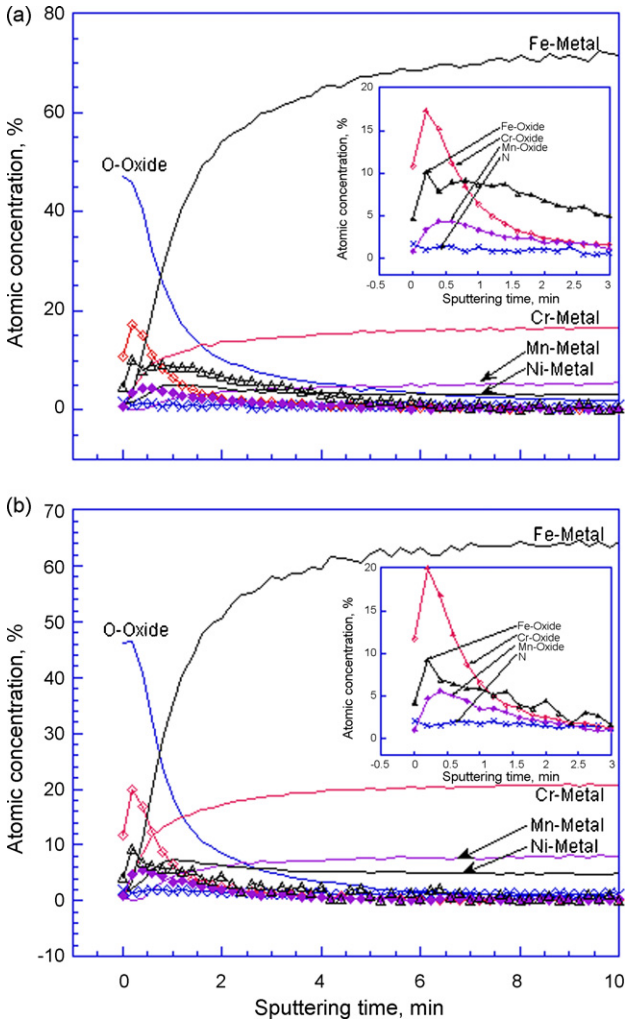

Fig. 9. XPS depth profiles for type 201 (a) and AL219 (b) steels after polarized 7.5 h at 0.6 V in 1 M H_2SO_4 + 2 ppm F^- solution of 70 °C. The solution was purged with air.

show long tails for both alloys. This is a significant difference from those films formed during polarization in the PEMFC anode environment, Fig. 8. The reason for this behavior is unknown. With a similar assumption of the oxygen in oxide, the passive film formed in the simulated PEMFC cathode environment is 3.4 nm for type 201 steel and 3.0 nm for AL219 steel. Regardless of the PEMFC environments, the passive film thickness are in the same range as the passive films formed on austenite stainless steels [18,24,26]. They are also in excellent agreement with the passive film thickness for most stainless steels treated under conditions identical to those of PEMFC bipolar plates [5].

4. Conclusions

Type 201 and AL219 stainless steels were investigated in 1 M H_2SO_4 + 2 ppm F^- solution at 70 °C purged either with hydrogen gas or pressurized air to simulate PEMFC environments for a bipolar plate application. Both steels exhibit better corrosion behavior than 316L steel in the same environments. Type 201 steel showed a similar but lower ICR than 316L, while AL219 steel showed a higher ICR than 316L.

The XPS analysis indicates that the air-formed films on Type 201 and AL219 are composed of iron oxides, chromium oxide, and manganese oxide. Iron oxides seem to dominate the composition

of the air-formed film, specifically the outer layer. On the other hand, the passive films were dominated by chromium oxide. The thickness of the surface films was calculated, and for the air-formed films depended on Ni content. N-alloying as a substitute for nickel appears to be promising for the PEMFC bipolar plate application of stainless steels.

Acknowledgements

The authors thank Mr. David J. McGhee of Allegheny Ludlum for the stainless steel samples. We also acknowledge Dr. Glenn Teeter for his assistant in the XPS investigation. This work was supported by the Hydrogen, Fuel Cells and Infrastructure Technologies Program of the U.S. Department of Energy.

References

[1] B.C.H. Steele, A. Heinzel, Nature 414 (2001) 345.
[2] R. Hornung, G. Kappelt, J. Power Sources 72 (1998) 20.
[3] P.L. Hentall, J.B. Lakeman, G.O. Mepsted, P.L. Adcock, J.M. Moore, J. Power Sources 80 (1999) 235.
[4] R.C. Makkus, A.H.H. Janssen, F.A. de Bruijn, R.K.A.M. Mallant, J. Power Sources 86 (2000) 274.
[5] D.P. Davies, P.L. Adcock, M. Turpin, S.J. Rowen, J. Appl. Electrochem. 30 (2000) 101.
[6] J. Wind, R. Späh, W. Kaiser, G. Böhm, J. Power Sources 105 (2002) 256.
[7] M.C. Li, C.L. Zeng, S.Z. Luo, J.N. Shen, H.C. Lin, C.N. Cao, Electrochim. Acta 48 (2003) 1735.
[8] S.-J. Lee, C.-H. Huang, J.-J. Lai, Y.-P. Chen, J. Power Sources 131 (2004) 162.
[9] H. Wang, M.A. Sweikart, J.A. Turner, J. Power Sources 115 (2003) 243.
[10] H. Wang, J.A. Turner, J. Power Sources 128 (2004) 193.
[11] H. Wang, G. Teeter, J.A. Turner, J. Electrochem. Soc. 152 (2005) B99.
[12] M.G. Fontana, N.D. Greene, Corrosion Engineering, 2nd ed., McGraw-Hill Book Company, New York, USA, 1978, 163 pp.
[13] H.H. Uhlig, R.W. Revie, Corrosion and Corrosion Control: An Introduction to Corrosion Science and Engineering, 3rd ed., John Wiley & Sons Inc., New York, USA, 1985, 78 pp.
[14] S.-L. Chou, M.-J. Tsai, W.-T. Tsai, J.-T. Lee, Mater. Chem. Phys. 51 (1997) 97.
[15] Y.S. Lim, J.S. Kim, S.J. Ahn, H.S. Kwon, Y. Katada, Corros. Sci. 43 (2001) 53.
[16] H. Baba, T. Kodama, Y. Katada, Corros. Sci. 44 (2002) 2393.
[17] H. Wang, M.P. Brady, K.L. More, H.M. Meyer III, J.A. Turner, J. Power Sources 138 (2004) 79.
[18] H. Wang, J.A. Turner, ECS Transactions, in: T. Fuller, C. Bok, C. Lamy (Eds.), Proton Exchange Membrane Fuel Cells V, in Honor of Supramaniam Srinivasan, vol. 1 (6) (2006) 263–272.
[19] S. Chou, M. Tsai, W. Tsai, J. Lee, Mater. Chem. Phys. 51 (1997) 97.
[20] R.D. Willenbruch, C.R. Clayton, M. Oversluizen, D. Kim, Y. Lu, Corros. Sci. 31 (1990) 179.
[21] D. Kim, C.R. Clayton, M. Oversluizen, Mater. Sci. Eng. A 186 (1994) 163.
[22] M.Z. Yang, J.L. Luo, Q. Yang, L.J. Qiao, Z.Q. Qin, P.R. Norton, J. Electrochem. Soc. 146 (1999) 2107.
[23] C.R. Clayton, G.P. Halada, J.R. Kearns, Mater. Sci. Eng. A 198 (1995) 135.
[24] D. Wallinder, J. Pan, C. Leygraf, A. Delblanc-Bauer, Corros. Sci. 41 (1999) 275.
[25] D. Stoychev, P. Stefanov, D. Nicolova, I. Valov, T.S. Marinova, Mater. Chem. Phys. 73 (2002) 252.
[26] S. Bera, S. Rangarajan, S.V. Narasimhan, Corros. Sci. 42 (2000) 1709.